Journal of Alloys and Compounds 507 (2010) 460–464

Contents lists available at ScienceDirect

Journal of Alloys and Compounds

journal homepage: www.elsevier.com/locate/jallcom

Molten salt synthesis, characterization and luminescence of $ZnWO_4$:Eu^{3+} nanophosphors

Bing Yan*, Fang Lei

Department of Chemistry, Tongji University, Siping Road 1239, Shanghai 200092, China

ARTICLE INFO

Article history:
Received 24 May 2010
Received in revised form 25 July 2010
Accepted 27 July 2010
Available online 4 August 2010

Keywords:
Optical materials
Oxide materials
Luminescence

ABSTRACT

$ZnWO_4$:Eu^{3+} red nanophosphors have been synthesized by a simple, environmentally friendly and low cost molten salt method using $LiNO_3$, $NaNO_3$ and KNO_3 as flux. We investigate the influences of the variety and amount of molten salt flux on photoluminescence properties of these phosphors. The products belong to the nanoparticle with particle size of around 50 nm. The PL intensity of the $ZnWO_4$:Eu^{3+} using $NaNO_3$ molten flux is stronger than that of the samples using KNO_3 molten flux, revealing that the remaining impurity molten salt produces the defects within $ZnWO_4$ host to be favorable for the luminescence of Eu^{3+}.

1. Introduction

AWO_4 type tungstates (A = Ca, Sr, Ba, Zn, Ni, Pb, Cd) have been extensively studied for their potential application in the fields such as phosphors, scintillation counter, laser and optic fiber [1–7]. Zinc tungstate ($ZnWO_4$), generally named assanmartinite, possesses the wolframite structure and crystallizes in the monoclinic system with space group $P2/c$, whose fundamental building units are [WO_6] and [ZnO_6] octahedron different from that of the common scheelite structure. The [ZnO_6] octahedron belongs to a distorted structure, in which two bond lengths are twenty percent longer than the other four [8]. $ZnWO_4$, as a kind of AWO_4 type tungstate, has attracted great interest for it can be used as X-rays and γ-rays scintillator, opto-electron anode, photocatalysis and solid-state laser. Besides, the low hygroscopicity of $ZnWO_4$ makes it more economic than other material such as $Bi_4Ge_3O_{12}$ (BGO), which is extensively used as scintillator materials. So it is urgent to require the high quality $ZnWO_4$ nanopowders [9–11].

AWO_4 functional materials have been prepared by various "soft-chemistry" routes, such as the solid-state reaction [12,13], hydrothermal method [14,15], microemulsion process [16], sol–gel process [17,18], molten salt method [19–21] and so on. Various synthesis procedures are developed for preparing certain functional micrometer or nanometer materials. Molten salt method has been extensively applied in the fields of electron ceramic powders and some other inorganic functional materials [22]. Molten salts can molten into ionic liquids at a relative low temperature, and have already been widely used as an effective chemical reaction medium to produce a high temperature liquid environment for crystal growth [23]. The ionic fluxes molten salts possess high reactivity toward different inorganic species and relatively low melting points which makes them convenient for preparation of inorganic materials. The molten salt synthesis (MSS) method is one of the simplest, most versatile, and cost-effective approaches available for obtaining crystalline, chemically purified, single-phase powders at lower temperatures and often in overall shorter reaction times with little residual impurities as compared with conventional solid-state reactions. The fundamental basis of molten salt reactions relies on the use of different types of inorganic molten salts as the reaction medium. As the reaction medium, the inorganic molten salts often possess a host of favorable physicochemical properties such as a greater oxidizing potential, high mass transfer, high thermal conductivity, as well as relatively lower viscosities and densities, as compared to conventional solvents [24]. Molten salt synthesis method is one effective way of preparing nano-scale shape-controlled materials in inorganic synthesis field [25–28]. Afanasiev had prepared barium molybdate and tungstate microcrystals with rhombic shape by molten flux reaction using alkali metal nitrates as reaction media [29]. We have also achieved the molten synthesis of Gd_2MO_6:Eu^{3+} (M = W, Mo) phosphors and found their microstructure is strongly related to the flux species [30].

In the context, a simple molten salt synthesis technology is engaged in the synthesis of homogenous controlled size $ZnWO_4$:Eu^{3+} nanosphere using alkali metal nitrates ($LiNO_3$, $NaNO_3$ and KNO_3) as the molten salts.

* Corresponding author. Tel.: +86 21 65984663; fax: +86 21 65982287.
E-mail address: byan@tongji.edu.cn (B. Yan).

0925-8388/$ – see front matter © 2010 Elsevier B.V. All rights reserved.
doi:10.1016/j.jallcom.2010.07.203

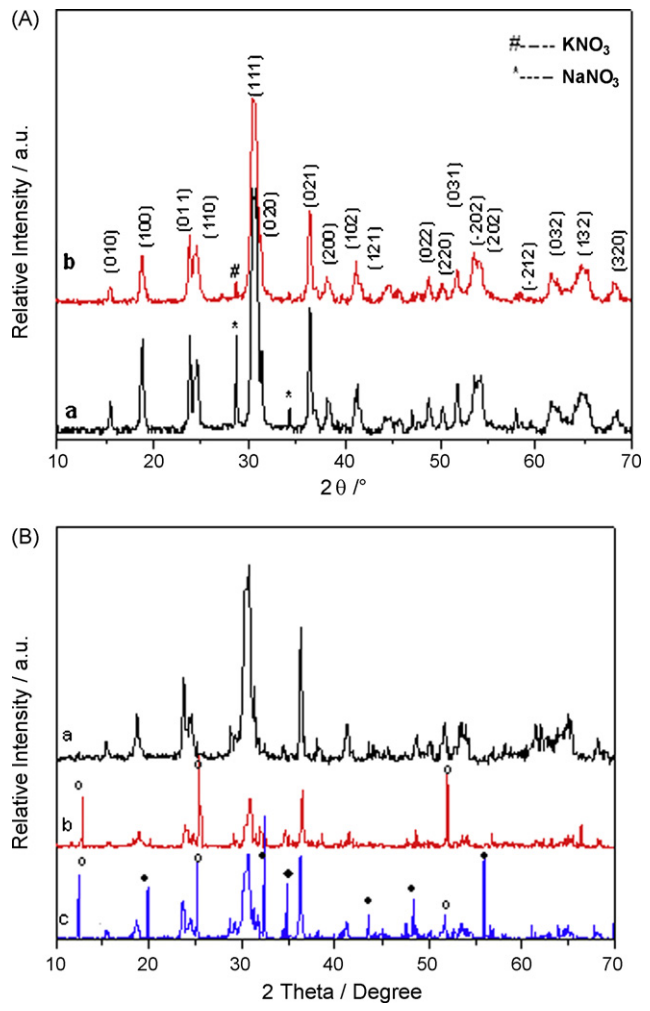

Fig. 1. The selected XRD patterns of $ZnWO_4$:Eu^{3+} using (a) $NaNO_3$ and (b) KNO_3 as molten salt (A) and using $LiNO_3$ as molten salt at 350 °C for (a) 1 h, (b) 4 h, and (c) 8 h (B).

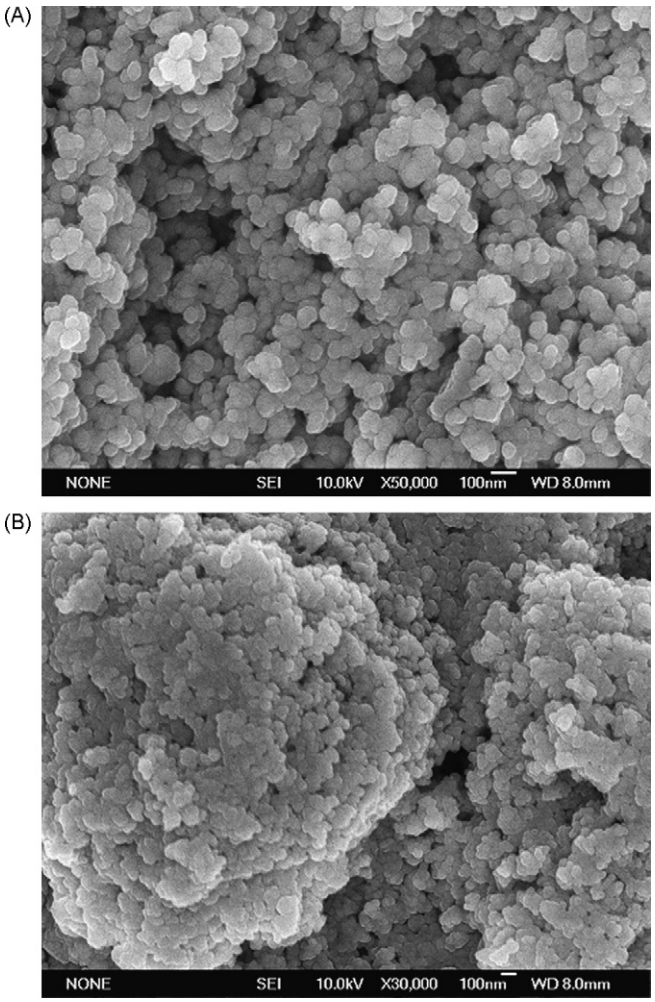

Fig. 2. The selected SEM images of $ZnWO_4$:Eu^{3+} using (A) $NaNO_3$ and (B) KNO_3 as molten salt.

2. Experimental

2.1. Chemicals

Starting materials ($Zn(NO_3)_2{\cdot}6H_2O$, $Na_2WO_4{\cdot}2H_2O$, $LiNO_3$, $NaNO_3$, KNO_3) are purchased from Aldrich and are used as received. Rare earth nitrates are prepared by dissolving their rare earth oxides with concentrated nitric acid.

2.2. Molten salt synthesis

In a typical MSS process, appropriate amounts of $Zn(NO_3)_2{\cdot}6H_2O$ and $Eu(NO_3)_2{\cdot}6H_2O$ are dissolved in the de-ionized water solution (15 mL), and 1 mmol $Na_2WO_4{\cdot}2H_2O$ is dissolved in the de-ionized water solution (5 mL). Then the two nitrate solutions are mixed by dipping and molten salts (MNO_3, M = Li, Na, K) are added further with molar ratio of Zn^{2+}:MNO_3 = 1:6. The mixed solution is heated to evaporate the water, then the product is put into the corundum crucible, and then calcined at 350 °C for 1–8 h. Finally, the products are cooled in the furnace to room temperature. The as-synthesized powders are thoroughly washed with deionized water for several times to ensure complete removal of the molten salt. The obtained products are further dried at 85 °C for 24 h.

2.3. Physical characterization

X-ray powder diffraction (XRD) analysis is carried out on a Bruker D8-Advanced X-ray diffractometer with high-intensity Cu Kα radiation (λ = 1.54 Å, 40 kV/60 mA, graphite monochromator). Thermogravimetric analysis is performed on a TG-DSC instrument (Netzsch STA-449C) at a heating rate of 10 K/min from 30 °C to a maximum temperature of 1000 °C. The morphology of the products is studied using environmental scanning electronic microscope (ESEM) (Philips XL-30). Transmission electron microscopy (TEM) equipped with an energy-dispersive X-ray spectra (EDS) is recorded on a JEOL200CX microscope with an accelerating voltage of 200 kV. Photoluminescence spectra are obtained by using RF-5301PC fluorescence spectrophotometer with Xe lamp at room temperature. FT-IR data are collected on Perkin–Elmer 2000 FT-IR spectrophotometer in the range of 400–7000 cm^{-1} using KBr pellets. UV–vis diffuse reflectance spectra (UV–vis DRS) of dry pressed disk samples are obtained on Lambda-900 UV–vis spectrophotometer and $BaSO_4$ is used as a reference standard.

3. Results and discussion

Fig. 1(A) shows the XRD patterns of $ZnWO_4$:Eu^{3+} phosphors synthesized by molten salt method at 350 °C for 5 h with different molten salts $NaNO_3$ (a) and KNO_3 (b), respectively, which indicates that these products are $ZnWO_4$ with remaining trace molten salts. Both of the X-rays diffraction peaks of $ZnWO_4$:Eu^{3+} from the two molten salts can be perfectly indexed to the monoclinic phase of $ZnWO_4$ (JCPDS 15-0774), belonging to space group $P2/c$ with lattice parameters of a = 4.691 Å, b = 5.72 Å, c = 4.925 Å, $\alpha = 90°$, $\beta = 90.64°$ and $\gamma = 90°$. The broadened diffraction peaks of the XRD patterns indicate the small crystal grain size of the products. The approximate particle sizes of Gd_2WO_6:Eu^{3+} and Gd_2MoO_6:Eu^{3+} can be calculated by the Debye–Scherrer's equation.

$$D = \frac{0.89\lambda}{\beta \times \cos\theta} \quad (1)$$

where D is the average grain size, λ represents the Cu Kα wavelength 0.1542 nm and β is the half-width. The mean particle sizes of

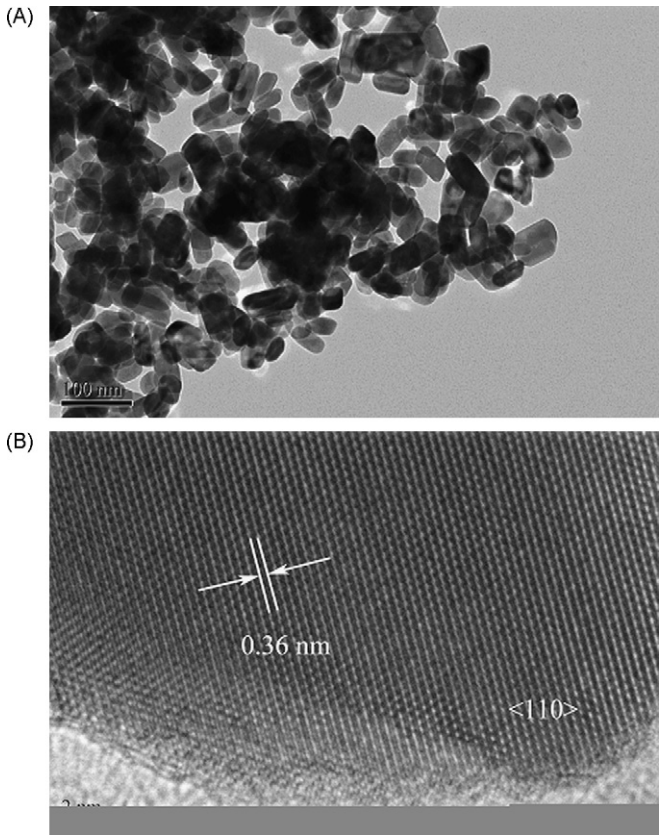

Fig. 3. The selected TEM (A) and HRTEM (B) images of $ZnWO_4$:Eu^{3+} using $NaNO_3$ as molten salt at 350 °C for 5 h.

$ZnWO_4$ samples using $NaNO_3$ and KNO_3 as molten salts are around 23 nm and 14 nm, respectively.

Further, we compare the XRD patterns of $ZnWO_4$:Eu^{3+} phosphors synthesized using $NaNO_3$ molten salt at 350 °C for different times: (a) 1 h, (b) 4 h and (c) 8 h, respectively (see Fig. 1(B)). All the X-rays diffraction peaks of $ZnWO_4$:Eu^{3+} can be perfectly indexed to the monoclinic phase of $ZnWO_4$ (JCPDS 15-0774), belonging to space group $P2/c$ and with lattice parameters of $a = 4.691$ Å, $b = 5.72$ Å, $c = 4.925$ Å, $\alpha = 90°$, $\beta = 90.64°$ and $\gamma = 90°$. With the increase of reaction time, the sharp diffraction peak of purity appears in the XRD pattern, which is identified as LiCl phase for the possible purity LiCl in the reactants. After reaction for 8 h, new unknown phase product can be observed, suggesting that the longer reaction time may produce the formation of hybrid phase. In this experiment, the aim product of $ZnWO_4$ can be obtained after 1 h.

Fig. 2(A) and (B) shows the selected SEM images of $ZnWO_4$:Eu^{3+} using $NaNO_3$ and KNO_3 as molten salt. Both of them present the homogenous nanometer particle size, whose average particle sizes are ~55 and ~50 nm, respectively. Fig. 3(A) and (B) illustrates the TEM and HRTEM images of $ZnWO_4$:Eu^{3+} using $NaNO_3$ as molten salt at 350 °C, which takes agreement with the results from SEM and presents the particle size of 50 nm. From the HRTEM image, the interplaner spacing is determined to be 0.36 nm, corresponding to the [1 1 0] crystal space.

Fig. 4 (A) shows the ultraviolet–visible reflectance absorption spectra of $ZnWO_4$:Eu^{3+} (A) using $LiNO_3$ as molten salt at 350 °C for different times: (a) 1 h, (b) 4 h, and (c) 8 h. It can be found that these samples show similar strong absorption band between 200 and 450 nm. One broad absorption band appears at the range of 200–350 nm, which is originated from the characteristic absorption of WO_4^{2-} group. Another wide shoulder absorption bands from 315 to 450 nm can be observed and may be due to the impurity in the products. Besides, the downward sharp peaks at 591, 596, 613, 624, 653 and 705 nm may be due to the self-

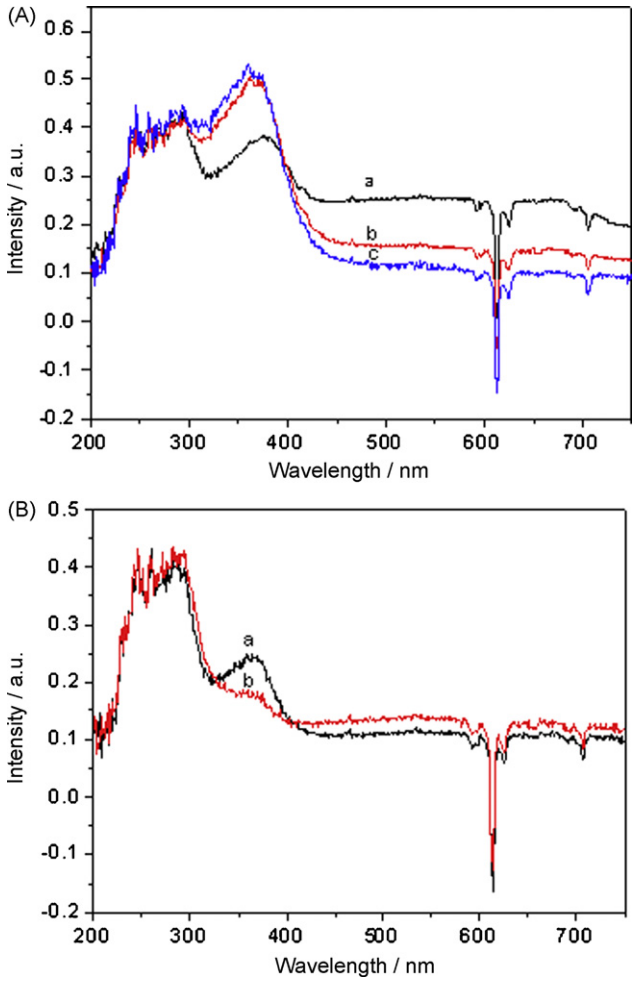

Fig. 4. The ultraviolet–visible reflectance absorption spectra of $ZnWO_4$:Eu^{3+} (A) using $LiNO_3$ as molten salt at 350 °C for different times: (a) 1 h, (b) 4 h, (c) 8 h and $ZnWO_4$:Eu^{3+} using (a) $NaNO_3$ and (b) KNO_3 as molten salt (B).

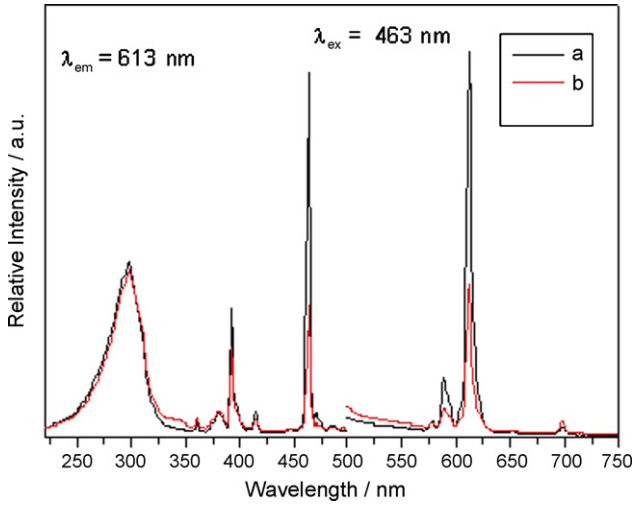

Fig. 5. Excitation and emission spectra of $ZnWO_4$:Eu^{3+} using (a) $NaNO_3$ and (b) KNO_3 as molten salt.

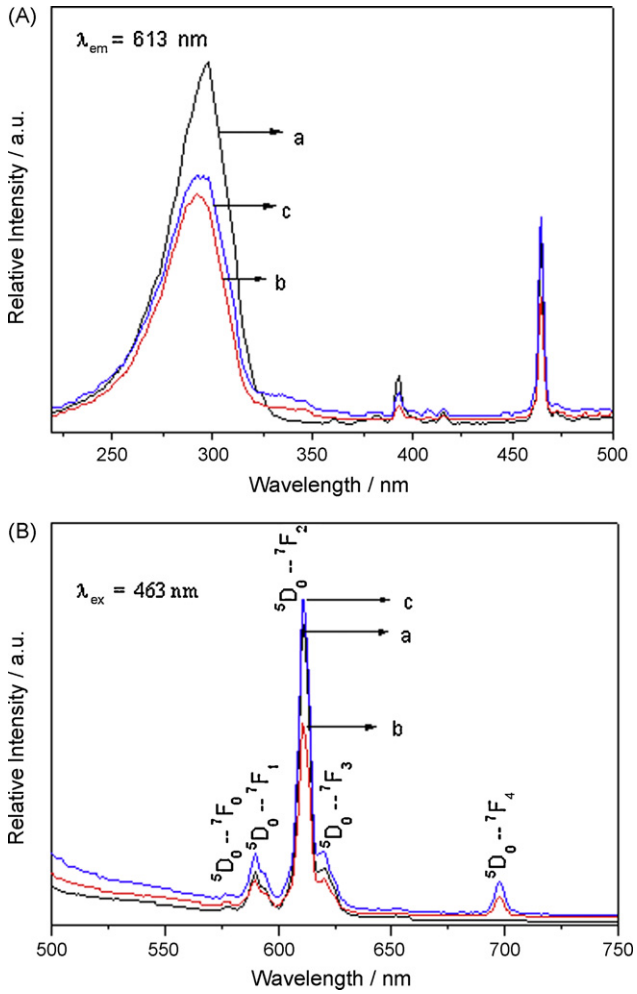

Fig. 6. Excitation (A) and emission (B) spectra of $ZnWO_4$:Eu^{3+} using $LiNO_3$ as molten salt at 950 °C for (a) 1 h, (b) 4 h, and (c) 8 h.

absorption of Eu^{3+} in the $ZnWO_4$ crystals. Fig. 4(B) compares the ultraviolet–visible reflectance absorption spectra of $ZnWO_4$:Eu^{3+} using different molten salts (a) $NaNO_3$ and (b) KNO_3, which shows the similar feature as above. It is worthy pointing out that the shoulder band of 320–425 nm of the product from KNO_3 shows the apparently weaker intensity than that from $NaNO_3$, which corresponds to the result of XRD pattern. The remaining molten salt impurity content of product from KNO_3 is much less than that from $NaNO_3$. So this further verifies that the wide shoulder band besides $O \rightarrow W$ CTS band is originated from the remaining molten salt impurity.

Fig. 5 wears the excitation and emission spectra of $ZnWO_4$:Eu^{3+} using (a) $NaNO_3$ and (b) KNO_3 as molten salt. The excitation spectra under 613 nm show broad excitation bands at the range of 220–350 nm with maximum peak of 297 nm, corresponding to the $O^{2-} \rightarrow W^{6+}$ charge transfer state (CTS) transition. Besides, the strong sharp excitation peaks can be observed at the long wavelength bands, 360, 380, 392, 415 and 463 nm, respectively, corresponding to the f–f transitions of Eu^{3+}, $^7F_0 \rightarrow {}^5D_4$, $^7F_0 \rightarrow {}^5L_7$, $^7F_0 \rightarrow {}^5L_6$, $^7F_0 \rightarrow {}^5D_2$, respectively. The corresponding emission spectra under the excitation of 463 nm present the characteristic emission peaks 576, 589, 611, 620, and 697 nm, respectively, which are attributed as the $^5D_0 \rightarrow {}^7F_J$ (J = 0, 1, 2, and 4) transition of Eu^{3+}. The dominated red peak comes from the hypersensitive transition $^5D_0 \rightarrow {}^7F_2$ with $\Delta J = 2$. This is a parity forbidden f–f intraconfigurational transition. When the Eu^{3+} is located at a low-symmetry local site (without an inversion center), the hypersensitive transition $^5D_0 \rightarrow {}^7F_2$ is often dominated in their emission spectra [31]. In addition, the emission intensity of the $ZnWO_4$:Eu^{3+} from $NaNO_3$ molten salt is higher than that from KNO_3. So it can be found that the suitable amount of purity in the products may produce some defects to become the new luminescent center, which is favorable for the luminescence of $ZnWO_4$:Eu^{3+}. Fig. 6 compares the excitation (A) and emission (B) spectra of $ZnWO_4$:Eu^{3+} using $LiNO_3$ as molten salt at 950 °C for different reaction times: (a) 1 h, (b) 4 h, and (c) 8 h, both of which present the similar feature as Fig. 5. The different reaction times have no apparent influence on the luminescent intensity of these products.

4. Conclusions

In summary, $ZnWO_4$:Eu^{3+} nanophosphors have been synthesized by a MSS technology at low temperature of 350 °C using $LiNO_3$, $NaNO_3$ and KNO_3 as molten salts. We believe the simple, environmentally friendly and low cost MSS method provides a convenient route for preparing nano-scale materials. These products show the particle size of around 50 nm. Using $LiNO_3$ as molten salt, pure phase $ZnWO_4$:Eu^{3+} crystal can be obtained after 1 h and then produces hybrid phase with the further increasing of time. The luminescent properties of $ZnWO_4$:Eu^{3+} are related to the fluxes of molten salts. The photoluminescent intensity of the as-prepared samples using $NaNO_3$ molten flux is stronger than the same product using KNO_3, which is due to fact that the remaining impurity molten salt produces the defects to be favorable for the luminescence of Eu^{3+}.

Acknowledgements

This work is supported by the Developing Science Funds of Tongji University and the National Natural Science Foundation of China (20971100).

References

[1] H.T. Shi, L.M. Qi, J.M.J.M. Ma, H.M. Cheng, J. Am. Chem. Soc. 125 (2003) 3450–3451.
[2] L.N. Sun, Q.R. Guo, X.L. Wu, S.J. Luo, W.L. Pan, K.L. Huang, J.F. Lu, L. Ren, M.H. Cao, C.W. Hu, J. Phys. Chem. C 111 (2007) 532–537.
[3] Y.G. Su, L.P. Li, G.S. Li, Chem. Mater. 20 (2008) 6060–6067.
[4] Q. Zhang, W.T. Yao, X.Y. Chen, L.P. Zhu, Y.B. Fu, G.B. Zhang, L.S. Sheng, S.H. Yu, Cryst. Growth Des. 7 (2007) 1423–1431.
[5] A.E. Troshin, V.E. Kisel, A.S. Yasukevich, N.V. Kuleshov, A.A. Pavlyk, E.B. Dunian, A.A. Komienko, Appl. Phys. B 86 (2007) 287–291.
[6] F. Zhang, Y. Yiu, M.C. Aronson, S.S. Wong, J. Phys. Chem. C 112 (2008) 14816–14824.
[7] Y.B. Mao, S.S. Wong, J. Am. Chem. Soc. 126 (2004) 15245–15252.
[8] J. Chi, J.C. Zang, W.L. Chu, J. Shandong Univ. Sci. Technol. 26 (2007) 60–64.
[9] G.L. Huang, S.C. Zhang, T.G. Xu, Y.F. Zhu, Environ. Sci. Technol. 42 (2008) 8516–8521.
[10] X. Zhao, Y.F. Zhu, Environ. Sci. Technol. 40 (2006) 3367–3372.
[11] H.J. Zhou, Y.B. Mao, S.S. Wong, Chem. Mater. 19 (2007) 5238–5249.
[12] C.Y. Xu, L. Zhen, R.S. Yang, Z.L. Wang, J. Am. Chem. Soc. 129 (2007) 15444–15445.
[13] T. Xu, X. Zhou, Z.Y. Jiang, Q. Kuang, Z.X. Xie, L.S. Zheng, Cryst. Growth Des. 9 (2009) 192–196.
[14] S. Neeraj, N. Kijima, A.K. Cheetham, Chem. Phys. Lett. 387 (2004) 2–6.
[15] X.X. Wang, Y.L. Xian, J.X. Shi, Q. Su, M.L. Gong, Mater. Sci. Eng. B 140 (2007) 69–72.
[16] F. Lei, B. Yan, J. Solid State Chem. 181 (2008) 855–862.
[17] Q. Gong, X.F. Qian, X.D. Ma, Z.K. Zhu, Cryst. Growth Des. 6 (2006) 1821–1825.
[18] M.L. Pang, X.M. Liu, J. Mater. Res. 20 (2005) 2676–2681.
[19] X.H. Jiang, J.F. Ma, J. Liu, Y. Ren, B.T. Lin, J.T. Tao, X.Y. Zhu, Mater. Lett. 61 (2007) 4595–4598.
[20] L.J. Xie, J.F. Ma, G.J. Xu, Mater. Chem. Phys. 110 (2008) 197–200.
[21] S.L. Ran, L. Gao, Chem. Lett. 35 (2006) 1312–1313.

[22] P.M. Rørvik, T. Lyngdal, R. Sæterli, A.T.J. van Helvoort, R. Holmestad, T. Grande, M.A. Einarsrud, Inorg. Chem. 47 (2008) 3173–3181.
[23] Z.Y. Cai, X.R. Xing, R.B. Yu, X.Y. Sun, G.R. Liu, Inorg. Chem. 46 (2007) 7423–7427.
[24] S.V. Volkov, Chem. Soc. Rev. 19 (1990) 21–28.
[25] J.H. Park, D.H. Lee, H.S. Shin, B.K. Lee, J. Am. Ceram. Soc. 19 (1996) 1130–1132.
[26] C.Y. Xu, Q. Zhang, H. Zhang, L. Zhen, J. Tang, L.C. Qin, J. Am. Chem. Soc. 127 (2005) 11584–11585.
[27] Y.B. Mao, T.J. Park, F. Zhang, H.J. Zhou, S.S. Wong, Small 3 (2007) 1122–1139.
[28] K. Teshima, K. Yubuta, S. Sugiura, Y. Fujita, T. Suzuki, M. Endo, T. Shishido, S. Oishi, Cryst. Growth Des. 6 (2006) 1598–1601.
[29] P. Afanasiev, Mater. Lett. 61 (2007) 4622–4626.
[30] F. Lei, B. Yan, H.H. Chen, J.T. Zhao, J. Am. Ceram. Soc. 92 (2009) 1262–1267.
[31] K. Riwotzki, M. Haase, J. Phys. Chem. B 105 (2001) 12709–12713.